A basic model for analysis of molten carbonate fuel cell behavior

Murat Baranak[a], Hüsnü Atakül[b,*]

[a] *TUBITAK Marmara Research Center, Institute of Energy, 41470 Gebze, Kocaeli, Turkey*
[b] *Istanbul Technical University, Department of Chemical Engineering, Maslak, Istanbul 34469, Turkey*

Abstract

A simple mathematical model, based on the basic chemical reactions and mass transfer, was developed to predict some important characteristics of molten carbonate fuel cells (MCFC) with $LiNaCO_3$ and $LiKCO_3$ electrolytes for steady state operating conditions. The parallel and cross gas flow patterns were analyzed. Model simulates polarization characteristics, the effect of temperature, pressure and electrolyte type on the cell performance, various losses in the cell and gas flow rate changes through cell. The effect of fuel utilization on the cell potential and efficiency was also analyzed. Model predicts a better performance for the MCFC with $LiNaCO_3$ electrolyte and the cross flow pattern, in general. Results show a strong influence of the operating temperature on the cell potential at temperatures below 625 °C, where cell potential increases rapidly with increasing temperature. Above this temperature, however, the cell potential has almost a steady asymptotic profile. The model predicts cell efficiency steadily improving with increase in fuel utilization. The cell potential decreases almost linearly with increase in the fuel utilization percentage for both electrolytes. Models results show a stronger dependency of the cell potential on the operating pressure than that described by the Nerst equation which is in line with fact that the real variations in the cell potential can be higher due to decreased various losses.
© 2007 Elsevier B.V. All rights reserved.

Keywords: Molten carbonate fuel cell; Model; Cell performance; Operating conditions

1. Introduction

Molten carbonate fuel cell (MCFC) is designed to operate at high temperature (>600 °C) and has already reached commercial scale with capacities of up to several megawatts. MCFC technology, with high efficiency and lower pollutant emissions, is expected to be used in stationary and distributed power generation applications [1]. MCFCs can achieve an efficiency of 60% stand-alone, or over 90% in case waste heat is used for cogeneration. This technology, however, is still in the developing stage and has not reached the commercial maturity to compete with the conventional energy conversion systems [2,3]. Challenges with MCFC are relatively slow oxygen reduction reaction, high bulkiness, the relatively low power density, corrosion, short cell lifetime and high cost. Advantages of this fuel cell are fuel flexibility and high operating temperature [2,4–6]. Fuel cells with high-power densities are needed to be developed in order to reduce the size and weight.

In parallel to the experimental studies, modeling and simulating studies have been going on to address many aspects related to the MCFC, such as better materials, better understanding of electrochemical processes and transport phenomena, better component and system design and the reduced voltage losses to overcome these problems. So far, many theoretical models of MCFC have been developed for various purposes [7–15]. One of the earliest elaborated studies of heat transfer characteristics of fuel cells and batteries was done by Baker [16]. Heat distribution in the MCFC has been covered by other model studies [7–9,17,18]. Kobayashi et al. [10] and Fujimura et al. [19] have developed models for temperature distribution prediction in a fuel cell stack with 12 cells. In these studies heat analysis based on the mass balance of the chemical reactions occurring in the cross flow type cells at atmospheric pressure. Similarly, in their modeling study Koh et al. [9,17] applied fluid dynamics and heat-transfer theories to predict dynamic pressure and temperature distribution in a co-flow molten carbonate fuel cell with an assumption of uniform current density. Computational fluid dynamics technique and numerical analysis have also been used to investigate performance of fuel cell stacks by calculation of three-dimensional distributions of crucial parameters [9,20–22].

* Corresponding author. Tel.: +90 212 285 68 57; fax: +90 212 285 34 25.
E-mail address: atakul@itu.edu.tr (H. Atakül).

Nomenclature

A_{unit}	area of a discrete unit
C_i	parameters related to electrodes and electrolytes
E	theoretically achievable maximum reversible potential (V)
E°	standard cell potential (V)
f	Faraday's constant (96,487 C equiv.$^{-1}$)
F	molar flow rate (mol h^{-1})
ΔG	the Gibbs free energy change (J mol^{-1})
ΔH	enthalpy (kJ kmol^{-1})
i	current (A)
j	current density (A m^{-2})
K_P	equilibrium constant
L	length of the fuel cell (cm)
P	partial pressure (bar)
R	resistance (Ω m^{-2})
R_{an}	irreversible losses at anode (Ω m^{-2})
R_{ca}	irreversible losses at cathode (Ω m^{-2})
R_{ir}	internal cell resistance (Ω m^{-2})
R_{tot}	the sum of irreversibility occurred at anode, cathode and electrode (Ω m^{-2})
T	temperature ($^\circ$C)
V	cell voltage (V)
x/L	dimensional x-axis
X	conversion degree
y/L	dimensional y-axis

Greek letter

η	loss

Subscripts

an	anode
ca	cathode
CO	carbon monoxide
CO$_2$	carbon dioxide
e	electrical
H$_2$	hydrogen
H$_2$O	water
i	species
i, an	species at anode
i, ca	species at cathode
ne	Nernst
tot	total

Superscript

o	standard

Abbreviations

CFD	computational fluid dynamics
LHV	lover heating value
LiNa	LiNaCO$_3$ electrolyte
LiK	LiKCO$_3$ electrolyte
MCFC	molten carbonate fuel cell
WGSR	water-gas shift reaction

On the other hand, unsteady-state modeling of a small-sized MCFC showed that the fuel cell may attain a steady-state very quickly, depending on the operational conditions [23,24]. It has been shown that model results may be an useful tool in evaluating the operation of the stack under transient conditions [22].

Simple models have been reported to producing reasonable predictions of fuel cell behavior that comparable to that of complex models [25,26].

In this paper, a simple basic model is introduced for MCFC with two different electrolytes for steady-state operating conditions. It is used to investigate the effects of basic parameters on the performance of fuel cell. We will discuss the effects of temperature and pressure on the cell voltage, changing of gas flow rates through the fuel cell and dependency of the efficiency on the fuel utilization.

2. Model formulation

A model was developed in order to investigate the effects of various parameters on the potential and the performance of the molten carbonate fuel cell (MCFC). This model also allows to evaluating the current density, efficiency losses and distribution of heat generated in the cell.
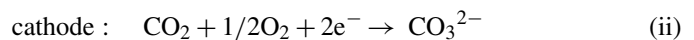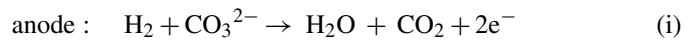
2.1. Model assumptions

The main model assumptions are:

- The reactant and products are ideal gas mixture.
- Plates are ideal conductor so that the voltage gradients through plates are negligible.
- Water-gas shift reaction taking place on the surface of the anode is fast and at equilibrium.
- Fuel cell operates isothermally.
- Pressure drop in the fuel cell is negligible.
- The cell operates under steady state conditions.

2.2. Chemical processes

The following electrochemical reactions are considered taking place in the electrodes of MCFC:

$$\text{anode}: \quad H_2 + CO_3{}^{2-} \rightarrow H_2O + CO_2 + 2e^- \qquad \text{(i)}$$

$$\text{cathode}: \quad CO_2 + 1/2O_2 + 2e^- \rightarrow CO_3{}^{2-} \qquad \text{(ii)}$$

$$\text{shift reaction}: \quad CO + H_2O \Leftrightarrow H_2 + CO_2 \qquad \text{(iii)}$$

The chemical process taking place in anode also includes the water-gas shift reaction via reaction (iii) which produces additional fuel (i.e., H$_2$) in the anode for fuel cell.

It is known from the fundamentals of the fuel cell that the efficiency of the fuel cell is inversely proportional to the current density. Since the plates, which are stainless steel, are assumed perfect conductor, the cell potential is almost constant. The total efficiency losses of this uniform-potential fuel cell can be determined depending on the current density and gas compositions. In this study the MCFC electrodes are assumed of being con-

sisted of discrete units where changes in the gas composition and current density can be neglected.

Various gas flow patterns are used in MCFC design. The most common ones are the parallel and cross flows. The anode and cathode gases flow in parallel and cross direction in the former and later one, respectively.

2.3. Approximate and governing equations

The operating cell potential (V) may be described as [5]

$$V = E - \eta_{ne} - jR_{tot} \tag{1}$$

where E is the theoretically achievable maximum reversible potential, η_{ne} is the Nernst loss, j is the current density, and R_{tot} is the sum of irreversibility occurred at anode, cathode and electrode. All unknowns and current densities in discrete units were calculated by using this equation. The sum of current densities of discrete units gives the total cell current. Eq. (1) is valid for all discrete units.

The maximum reversible potential of fuel cells is obtained from the Gibbs free energy change of hydrogen oxidation reaction:

$$E = \frac{-\Delta G}{2f} \tag{2}$$

where ΔG is the Gibbs free energy and f is the Faraday constant. The Gibbs free energy change may be expressed as function of temperature by [27],

$$-\Delta G = -242000 + 45.8T \tag{3}$$

where T is the temperature (K).

The standard cell potential is obtained from Gibbs free energy of reaction. The second term on right hand of Eq. (2) is the Nernst loss described by [2],

$$\eta_{Nernst} = \frac{RT}{2f} \ln \left[\frac{P_{H_2,an}(P_{O_2,ca})^{1/2} P_{CO_2,ca}}{P_{H_2O,na} P_{CO_2,an}} \right] \tag{4}$$

The total irreversible losses, R_{tot}, consist of over potentials and cell resistance:

$$R_{tol} = R_{an} + R_{ca} + R_{ir} \tag{5}$$

where R_{an} and R_{ca} are irreversible losses of anode and cathode, respectively, and R_{ir} is the internal cell resistance. Losses for MCFCs may be calculated by the following equations [28]:

$$R_{an} = C_a \, e^{\Delta H_a/RT} P_{H_2,an}^{-0.5} \tag{6}$$

$$R_{ca} = (C_1 \, e^{\Delta H_{C_1}/RT} P_{O_2,ca}^{-0.75} P_{CO_2,ca}^{0.5})$$
$$+ (C_2 \, e^{\Delta H_{C_2}/RT} C_{CO_2,ca}^{-1}) \tag{7}$$

$$R_{ir} = C_{ir} \, e^{\Delta H_{ir}/RT} \tag{8}$$

where R is the resistance ($\Omega \, cm^{-2}$), C_i the parameter related to electrodes and electrolytes, P the pressure (atm) and ΔH the enthalpy (J mol^{-1}). These equations indicate that, irreversible losses at electrodes depend on temperature, pressure, partial pressures of gases, H_2 at anode, CO_2 and O_2 at cathode, and some parameters related to electrodes and electrolytes. The cell internal resistance depends on the ionic conductivity of the electrolyte and electrical conductivity of the plates.

The equilibrium state described by Eq. (1) is attained in all discrete units. The cell potential (V) is constant, but E, η_{ne}, and R_{tot}, however, change from inlet to outlet along the cell surface due to the decrease of gas concentrations or their partial pressures. Accordingly, the current density changes simultaneously along the cell surface. The current density (j) for each discrete unit is determined by,

$$j = \frac{E - V - \eta_{ne}}{R_{tol}} \tag{9}$$

The current (i) in a discrete unit is obtained as the product of the current density and surface area:

$$i = jA_{unit} \tag{10}$$

where A_{unit} is the area of a discrete unit, 80 cm^2, which is 1/25 of the total cell area of 2000 cm^2. The cell is considered in square shape. The produced current is proportional to amount of the reactants consumed in the reactions. Relationships between the current and gas molar flow rates are defined by the following equations:

$$\Delta F_{H_2,an} = -0.018655i \tag{11}$$

$$\Delta F_{CO_2,ca} = -0.018655i \tag{12}$$

$$\Delta F_{O_2,ca} = -0.0093275i \tag{13}$$

$$\Delta F_{H_2O,an} = 0.018655i \tag{14}$$

$$\Delta F_{CO_2,an} = 0.018655i \tag{15}$$

where $\Delta F_{i,an}$ and $\Delta F_{i,ca}$ are the molar flow rate changes of species i at anode and cathode, respectively. The coefficients in these equations are described as mol i h^{-1} A^{-1}.

Water-gas shift reaction (WGSR) taking place on the nickel catalyst at high temperatures is very fast and rapidly reaches to the equilibrium. Decrease in the hydrogen concentration and increase in the water and carbon dioxide concentrations leads to a non-equilibrium state in this reaction.

The equilibrium constant (K_P) for WGSR is described based on thermodynamic by,

$$K_P = \frac{P_{CO_2} P_{H_2}}{P_{CO} P_{H_2O}} \tag{16}$$

The following equation was used to describe the relationship between the equilibrium constant of WGSR and temperature [28]:

$$\ln(K_P) = \frac{4276}{T} - 3.961 \tag{17}$$

For a conversion degree of X, the equilibrium constant (K_P) is obtained as:

$$K_P = \frac{(P_{CO_2} + X)(P_{H_2} + X)}{(P_{CO} - X)(P_{H_2O} - X)} \tag{18}$$
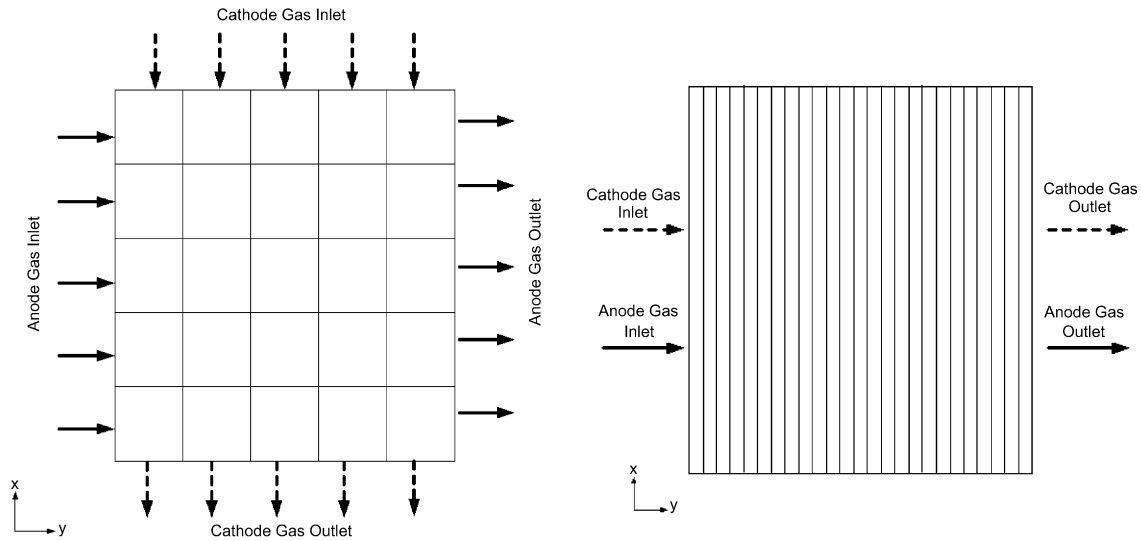
Fig. 1. Schematic of computational domain of MCFC electrodes. (a) Cross-gas flow and (b) parallel-gas flow.

The partial pressure of gases is described by,

$$P_i = \frac{F_i}{F_{tot}} P_{tot} \tag{19}$$

where P_i is the partial pressure of species i, P_{tot} is the total pressure, F_i is the molar flow rate of species i and F_{tot} is the total molar flow rate of the gas mixtures. All species have the same P_{tot} and F_{tot} values. Rearrangement of Eq. (18) leads to the following equation:

$$(1 - K_P)X^2 + [F_{H_2} + F_{CO_2} + K_P(F_{CO} + F_{H_2O})]X$$
$$+ [(F_{CO_2}F_{H_2}) - (F_{CO}F_{H_2O})K_P] = 0 \tag{20}$$

Solution to this equation gives molar flow rates of gases as a function of conversion:

$$F_{H_2} = F_{H_2} + X \tag{21}$$

$$F_{CO_2} = F_{CO_2} + X \tag{22}$$

$$F_{CO} = F_{CO} - X \tag{23}$$

$$F_{H_2O} = F_{H_2O} - X \tag{24}$$

The solutions of the last four equations, Eqs. (21)–(24), give the outlet composition of a discrete unit under consideration and the inlet compositions of the next one. Changes in the compositions of the anode and cathode gas streams were studied for both parallel and cross flows cases. In parallel flow, in which the anode and cathode gas streams flow in the same direction, inlet and outlet compositions of a unit can relatively easily be described. But in cross flow, the situation is more complex. In this study, we have written a computer code to solve the equations that describe the composition profiles of gas streams.

The total amount of electrical current produced in fuel cell (i_{tot}) is calculated as the summation of the current produced in the discrete units:

$$i_{tot} = \sum i \tag{25}$$

2.4. Numerical solution

The fuel cell, 2000 cm^2, is discretized into solution domains for cross- and parallel-gas flow cases that are schematically depicted in Fig. 1 and considered for numerical solution. The cell potential, which is a function of various parameters and changes from unit to unit, is determined by using an iteration method. For solution, the model equations described above are applied for each discrete unit. The model equations' solutions for discrete units require a known whole cell operating potential. Operating voltage is assumed to be constant within the cell, since the separator plates are well conductors and the voltage losses along the plates are negligible. An initial value for the cell potential, V, was assigned to start the solution process. The current density and the flow rates of gases in each unit in the cell were calculated according to the Eqs. (1)–(24). The total current of the cell was calculated by Eqs. (10) and (25). This result was compared with value of total current which was calculated depending on the fuel feeding rate and fuel utilization ratio. Iteration process was repeated with changing the cell potential values till the difference between the values of these current values satisfied a desired error tolerance, so that the solution is obtained.

The operating conditions of the cell used in the model are listed in Table 1. The anode and cathode inlet gas compositions were determined by using ASPEN HYSYS 3.2 process simulating software. The numerical values of parameters involved in

Table 1
Operating conditions considered in the model

Gases	Anode inlet (%)	Cathode inlet (%)
H$_2$	26.60	–
CO	4.40	–
CO$_2$	10.70	12.90
Water vapor	34.00	29.20
O$_2$	–	5.70
N$_2$	24.30	52.20

Table 2
Parameters in performance equations (Eqs. (6)–(8))

Parameter	LiNaCO$_3$$^{-2}$	LiKCO$_3$$^{-2}$
C_1	3.28×10^{-9}	1.97×10^{-6}
C_2	3.39×10^{-6}	2.2×10^{-3}
C_a	2.04×10^{-3}	1.39×10^{-6}
C_{ir}	1.12×10^{-2}	0.0128
ΔH_{C_1} (J mol^{-1})	132,000	83,400
ΔH_{C_2} (J mol^{-1})	67,100	22,800
ΔH_a (J mol^{-1})	23,700	77,800
ΔH_{ir} (J mol^{-1})	23,000	25,200

Eqs. (6)–(8) are basically adopted from [28] and presented in Table 2.

3. Results and discussions

In this section the polarization (*V–I*) curve, the predicted results of various losses in the fuel cell, the effects of operating temperature and pressure on cell potential, changes in the flow rates of H$_2$, O$_2$, CO and CO$_2$ through the fuel cell, the effect of fuel utilization on fuel cell potential and the fuel cell efficiency are reported. These predicted results have been produced for both LiNaCO$_3$ and LiKCO$_3$ types molten carbonate fuel cells with parallel gas flow regime. Lastly, the predicted polarization curve of molten carbonate with LiNaCO$_3$ will be presented for both parallel and cross gas flow.

3.1. Prediction of the MCFC performance curve

The model was used to investigate the effects of various operating parameters on the performance of a MCFC. The parameters considered are operating temperature and pressure, current density, fuel utilization, gas flow type and electrolyte types. LiNaCO$_3$ and LiKCO$_3$ were considered as electrolytes in the modeling.

The polarization curve, also known as performance curve, is one of the most useful tool to characterize the behavior of a fuel cell. The characteristic polarization curves produced by the model for MCFC with LiNaCO$_3$ and LiKCO$_3$ electrolytes are shown in Fig. 2. Results obtained from the model are in parallel
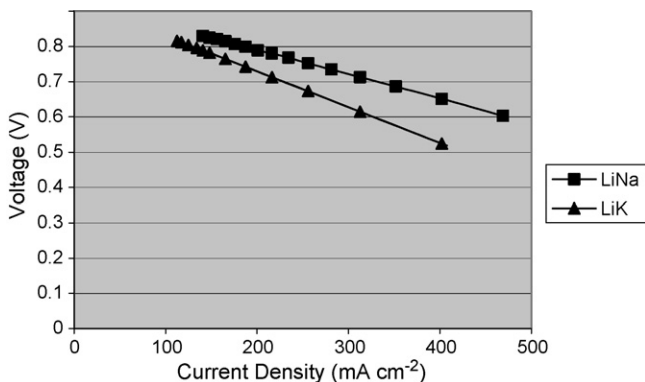

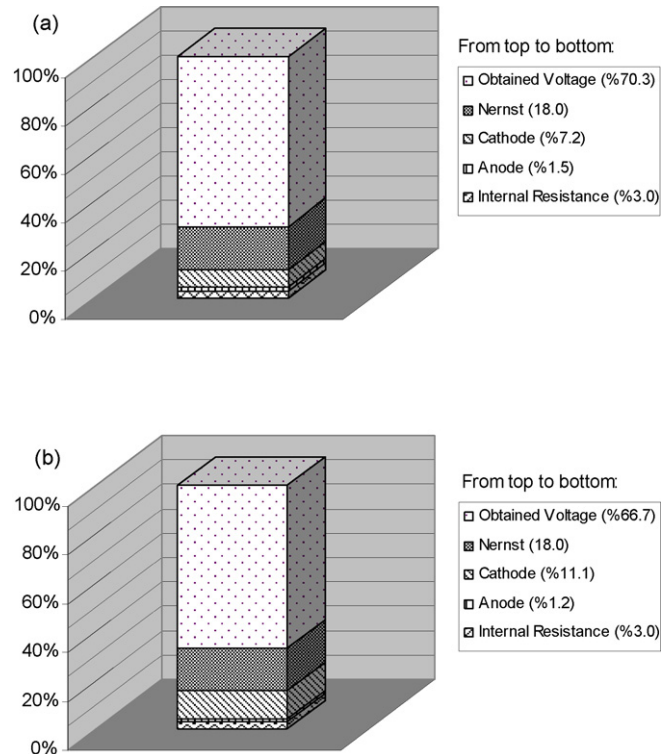Fig. 2. Polarization curves of molten carbonate fuel cells with LiNaCO$_3$ and LiKCO$_3$ electrolytes.

Fig. 3. Various losses and net potential value of molten carbonate fuel cells. (a) MCFC with LiNaCO$_3$ electrolyte and (b) MCFC with LiKCO$_3$ electrolyte.

with data given in the literature, which state that the operating potential of a fuel cell decreases with increasing current density [29,30]. This is an expected result, since the anode, cathode and electrolyte irreversibilities are proportional to current density. In the operating range considered in this study, a linear relationship is observed between operating potential and current density for both electrolytes. However, the operating potential of LiNaCO$_3$ electrolyte fuel cell is higher than that of LiKCO$_3$ electrolyte fuel cell and gap between the potentials of two electrolytes becomes more clear at high current densities. This behavior indicates that LiNaCO$_3$ electrolyte fuel cells are comparatively more efficient.

Various losses and net potential values predicted by the model in the fuel cell are compared in Fig. 3 for both LiNaCO$_3$ and LiKCO$_3$. This figure was produced based on a 140 mA cm^{-2} average current density. The net potential values of the fuel cells were calculated by subtraction of the total loss from the theoretical maximum reversible potential. Comparison of Fig. 3a and b reveals, in general, a similar picture for both electrolytes. The internal cell resistance and cathode losses of the LiNaCO$_3$ are smaller than those of LiKCO$_3$. The predicted difference between the internal resistances of the fuel cells, which represents the electrolyte resistance to ionic conduction, may be attributed to their ionic conductions which are 2.40 Ω cm^{-1}, and 1.60 Ω m^{-1} for the former and latter, respectively. Although the anode and cathode losses are known originating from activation, mass transfer and concentration losses, and their relationship with reaction mechanisms have still not been well established. The lower cathode loss of LiNaCO$_3$ is likely due to the higher solubility of carbon dioxide in this electrolyte. On the other hand,
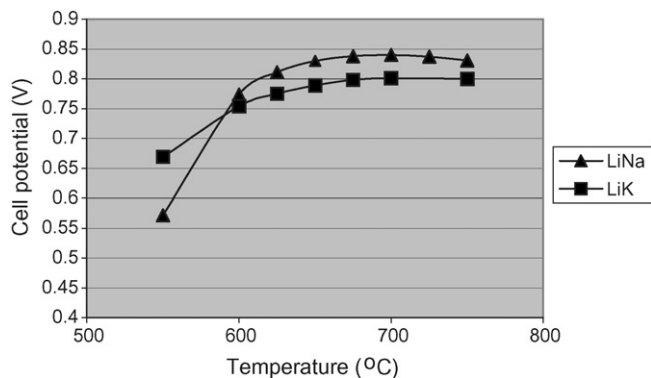
Fig. 4. Effect of temperature on the molten carbonate fuel cell potential.

oxygen solubility of the $LiKCO_3$ electrolyte is higher than that of $LiNaCO_3$. But carbon dioxide solubility has a stronger influence on the cathode polarization.

3.2. Prediction of the temperature effect on the MCFC performance

The temperature dependency of the cell potentials predicted by the model is plotted in Fig. 4 for both electrolytes. The figure shows a strong influence of the operating temperature on the cell potentials at temperatures below 625 °C, with cell potentials increasing rapidly with increasing temperature. Although, the thermodynamic calculations showed that the operating cell potential, and consequently the cell efficiency, may improve as temperature increases, above this temperature level the cell potentials reach almost steady asymptotic values after which they do not change considerably. MCFC systems commonly operate in the temperature range of 600–700 °C. Therefore, the model predictions, indicating that the maximum cell potentials are obtained in this temperature range, suit well with data obtained from experimental studies in this respect [2,30]. Curves in the figure also compare the performances of the two fuel cell types based on relation between cell potential and temperature and show that the MCFC with $LiNaCO_3$ electrolyte produces slightly higher potential than the MCFC with $LiKCO_3$ electrolyte at temperatures higher than 575 °C (575–750 °C), the temperature range in which MCFCs commonly operate. Below this temperature, however, the later one appears to have a better efficiency. This may be attributed to the solubility of the oxygen which decreases faster with increasing temperature for $LiNaCO_3$. A temperature of 650 °C appears to the optimum operating temperature for both fuel cells as the vaporization of electrolytes increases and corrosion of separating plates enhances considerably above this temperature level while operating voltage remains constant. Above 650 °C, however, the dependency of cell potential on the operating temperature fades away.

3.3. Prediction of the pressure effect on the MCFC performance

Operating pressure has been involved in the operating parameters that can considerably affect the performance of the MCFC.
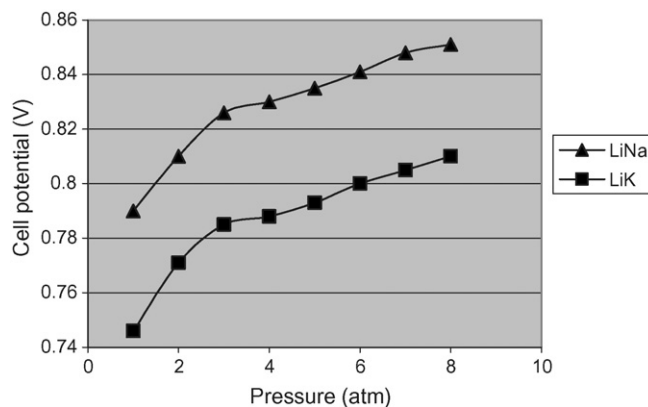

Fig. 5. Effect of pressure on the molten carbonate fuel cell potential, $T = 650$ °C.

Variations of the cell potentials of the MCFC with operating pressure obtained from model are depicted in Fig. 5. As seen from the figure, the cell potentials steadily increase with increase in the operating pressure for both electrolytes. Increase in pressure results in higher cell voltages due to the increased partial pressure of gases and improved gas solubility and mass transport characteristics of the cell [2].

The model results suggest a stronger dependency of the cell potential on the pressure in comparison with that described by the Nernst equation. According to the Nernst equation, an eight-fold increase in pressure results in an increase of 41.6 mV in the reversible cell potential at 650 °C, while an increase of approximately 60 mV is calculated in this study for both MCFCs. This stems from the fact that the real variation in the cell potential is higher than that calculated from the Nernst equation due to the decreased overpotentials consisting of anode, cathode and internal losses.

The MCFC with $LiNaCO_3$ electrode is clearly superior to the MCFC with $LiKCO_3$ electrode. Both fuel cells, however, display similar trends in the potential variation, a stronger dependency on pressure up to 3 atm and a relatively weaker dependency after that. These data are in consistent with results previously presented in Figs. 2 and 4 and also indicate a better performance for the MCFC with $LiNaCO_3$ electrolyte in respect to the performance curve and the cell potential.

3.4. Gas flow rates and the effect of the fuel utilization percentage on MCFC performance

The gas flow rate changes in the flow direction in the anode and cathode, predicted by the model, are shown in Fig. 6, and Fig. 7, respectively. These figures were produced for the $LiNaCO_3$ electrolyte MCFC and cross flow regime. The hydrogen flow rate, as expected, decreases in the flow direction as it is consumed by anode reactions as shown in Fig. 6a. On the other hand, as seen in Fig. 6b, in parallel to hydrogen consumption, carbon monoxide also depletes along the flow direction as a result of the water-gas shift reaction which results in hydrogen production. Consequently, change in hydrogen flow rate becomes slower while an inverse trend is observed for the
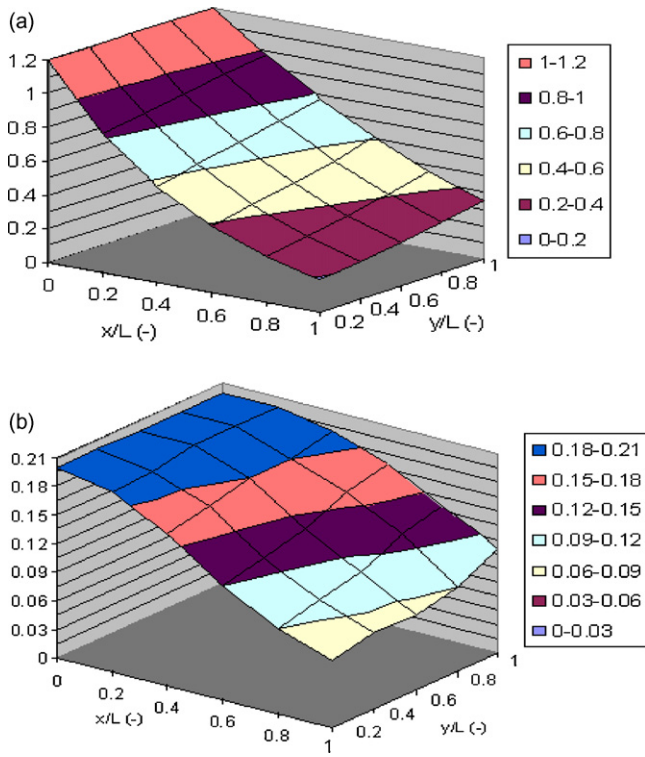
Fig. 6. Changing of gas flow rate through the anode of a molten carbonate fuel cell with cross flow and LiNa CO₃ electrolyte. (a) H_2 and (b) CO.

carbon dioxide. Contrary to the anode, in the cathode oxygen and carbon dioxide flow profiles are similar, both indicating a steady decrease in flow rates of both gases, as may be seen from Fig. 7. These profiles are in good agreement with the chemical process taking place in the cathode, in which both oxygen and carbon dioxide are consumed.

In Fig. 8, the cell potential is plotted as function of the fuel utilization percentage. The cell potential drops almost linearly with increase in the fuel utilization percentage for both electrolytes. This fits well with the fact that cell current density increases in parallel to the fuel utilization degree and the Nernst loss increases as concentrations of species in electrodes decrease. Both phenomena result in a decrease in the cell potential.

Conversion efficiency is one of the most important factor affecting the fuel cell performance. Here, we define the cell efficiency as the ratio of the total dc power produced in the cell to the LHV of total fuel, hydrogen and carbon monoxide, supplied to the cell. This is the gross fuel cell efficiency. The model prediction of the relationship between the cell efficiency and the fuel utilization percentage is plotted in Fig. 9. The cell efficiency steadily improves as the fuel utilization increases. Although, high fuel utilization looks favorable for cell operation, it should be noticed that the cell efficiency improvement remains limited at high utilization degrees. Therefore, it might be possible to improve the overall efficiency of an integrated fuel processor-fuel cell system by operating the cell at moderate fuel utilization (75–80%) and feeding the remaining unused fuel to a combustor for heat production.
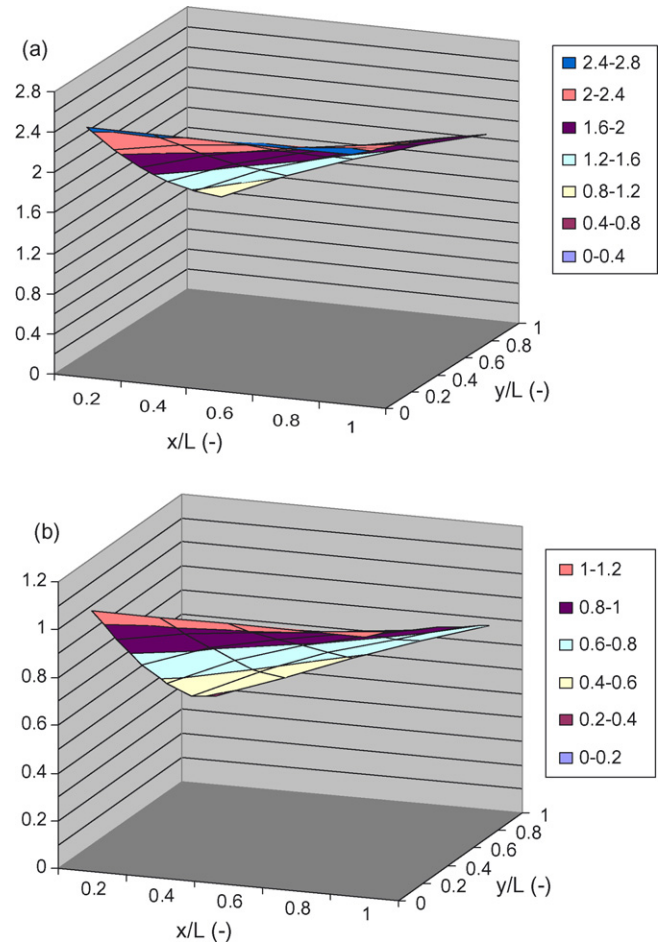

Fig. 7. Changing of gas flow rates through the cathode of a molten carbonate fuel cell with cross flow and LiNa CO₃ electrolyte. (a) CO_2 and (b) O_2.

3.5. Prediction of the effect of flow type on the MCFC performance

Various types of gas flow configuration are used in the MCFCs design. The parallel flow, in which the anode and cathode gases flow in the same direction, and the cross flow, in which the anode and cathode gases flow in cross direction, are commonly used in the design of MCFC systems. The polar-
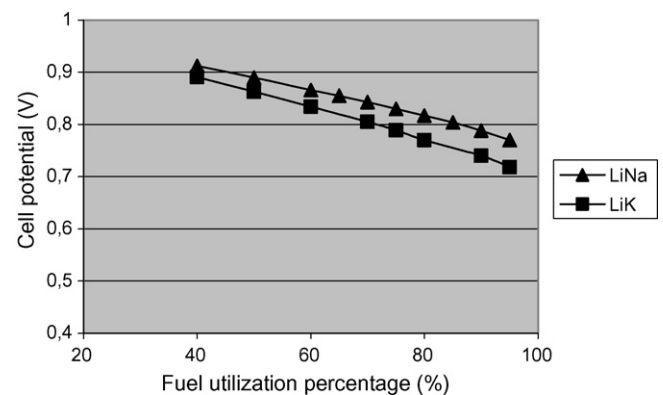

Fig. 8. Cell potential as function of the fuel utilization percentage in the molten carbonate fuel cells with LiNaCO₃ and LiKCO₃ electrolytes.
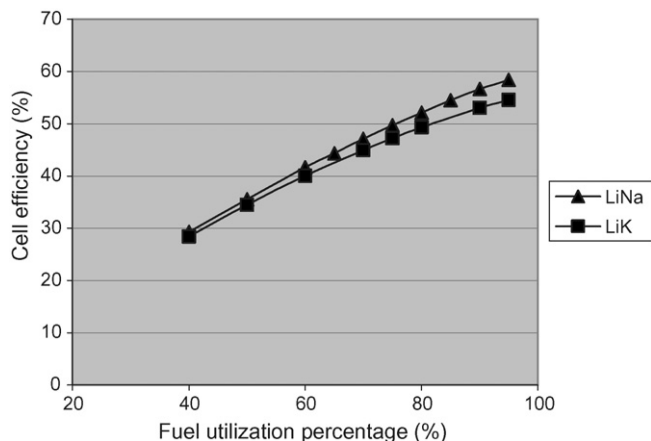
Fig. 9. Cell efficiency as function of the fuel utilization percentage in the molten carbonate fuel cells with $LiNaCO_3$ and $LiKCO_3$ electrolytes.

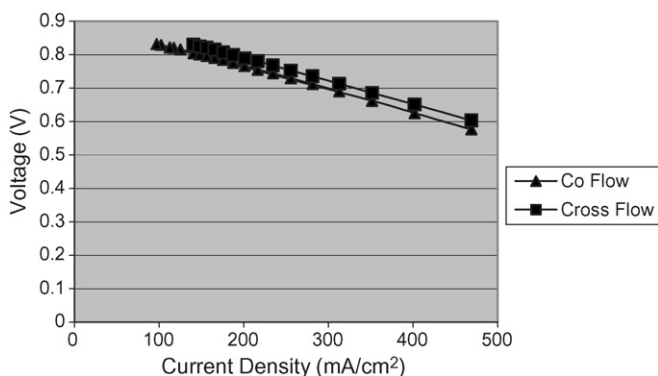Fig. 10. Polarization curves of molten carbonate fuel cells with parallel and cross gas flows. Electrolyte: $LiNaCO_3$, $T = 650\,°C$, $P = 3.5$ bar.

ization curves of the $LiNaCO_3$ electrolyte MCFC produced via the model for both flow configurations are presented in Fig. 10 for 650 °C and 3.5 bar operating conditions. Although both flow configurations produce similar cell voltage curves, the cell voltage and, consequently efficiency, are little higher in cross flow case. Different conclusions have been reported in the literature about the relations between MCFC performance and flow types. Predictions in Fig. 10 are in agreement with results obtained by Wolf and Wilemski, [8], indicating that cross flow had a better performance than the co-flow type stacks in terms of cell voltage and current relation. These predictions, however, are not in line with model results of Yoshida et al. [21], who reporting the co-flow type stack to have the highest net output power in the five gas flow type stacks they studied. In addition to higher efficiencies, MCFCs with cross flow pattern have further advantages such as lower pressure loss, even gas distribution and simple design.

4. Conclusions

A mathematical model, depending on the chemical processes involved, has been developed for the steady state molten carbonate fuel cells with $LiNaCO_3$ and $LiKCO_3$ electrolytes. The behavior of the fuel cells, in terms of flow patterns, the perfor-

mance curve, effects of temperature, gas flow rates, and fuel utilization on the cell performance curve, prediction of various losses, changes of gas flow rates through anode and cathode, relationship between the cell potential and the fuel utilization, dependency of the cell efficiency on the fuel utilization, were investigated and the followings are concluded:

In general, molten carbonate fuel cell with $LiNaCO_3$ electrolyte has a better performance than the fuel cell with $LiKCO_3$ electrolyte, but both fuel cells have similar behaviors in respect of effects of various operating parameters considered in the study. On the other hand, the performance of the fuel cell with cross gas flow is slightly better than that of the fuel cell with parallel gas flow.

The operating temperature strongly affect the cell potential below temperature of about 625 °C, where cell potential increases with increasing temperature. Above this temperature level, however, the cell potential retains a steady and asymptotic pattern with no considerable changes.

The cell potential inversely and almost linearly changes with the fuel utilization percentage. The model, however, predicts a steadily improving cell efficiency with increase in the fuel utilization and decease in the gas flow rates in both anode and cathode.

The model results also indicate a relatively strong dependency of cell potential on the operating pressure. The cell potential increases with increase in operating pressure for both MCFC with $LiNaCO_3$ and MCFC with $LiKCO_3$ electrolydes. The potential values predicted by the model, however, are higher than that obtained from the Nernst equation.

References

[1] P.B. Tarman, J. Power Sources 61 (1996) 87–89.
[2] K. Kordesch, G. Simader, Fuel Cells and Their Applications, VCH, New York, 1996, pp. 111–113.
[3] B.P. Bos, J. Power Sources 61 (1996) 21–31.
[4] A. Hamnett, in: A. Vielstich, H.A. Lamm, Gasteiger (Eds.), Handbook of Fuel Cells, Fundamentals, Technology and Applications, vol. 4, Wiley, New York, 2003, pp. 36–43.
[5] Y. Mugikura, in: W. Vielstich, A. Lamm, H.A. Gasteiger (Eds.), Handbook of Fuel Cells, Fundamentals, Technology and Applications, vol. 4, Wiley, New York, 2003, pp. 907–920.
[6] J. Hoffmann, C.Y. Yuh, A.G. Jopek, in: W. Vielstich, A. Lamm, H.A. Gasteiger (Eds.), Handbook of Fuel Cells, Fundamentals, Technology and Applications, vol. 4, Wiley, New York, 2003, pp. 921–941.
[7] V. Sampath, A.F. Sammels, J.R. Selman, J. Electrochem. Soc. 127 (1980) 79–85.
[8] T.L. Wolf, G. Wilemski, J. Electrochem. Soc. 130 (1983) 48–55.
[9] J.H. Koh, B.S. Kang, H.C. Lim, AIChE J. 47 (2001) 1941–1956.
[10] N. Kobayashi, H. Fujimura, K. Ohtsuka, J. Jpn. Mech. Eng. Int. 32 (1989) 420.
[11] B. Bosio, P. Costamanga, F. Paradi, Chem. Eng. Sci. 54 (1999) 2907–2916.
[12] Y.R. Lee, M.J. Yoo, G.Y. Chung, H.C. Lim, T.H. Lim, S.W. Nam, S.A. Hong, Kor. J. Chem. Eng. 22 (2005) 219–227.
[13] F. Yoshiba, T. Abe, T. Watanabe, J. Power Sources 87 (2000) 21–27.
[14] M. Mangold, M. Sheng, Fuel Cells 4 (2004) 68–77.
[15] H. Hirata, M. Hori, J. Power Sources 63 (1996) 115–120.
[16] B.S. Baker, Heat transfer in electrochemical systems, Ph.D Thesis, Illinois Institute of Technology, 1969.
[17] J.H. Koh, H.K. Seo, Y.S. Yoo, H.C. Lim, Chem. Eng. J. 87 (2002) 367–379.
[18] J.H. Koh, B.S. Kang, H.C. Lim, J. Power Sources 91 (2000) 161–171.

[19] H. Fujimura, N. Kobayashi, K. Ohtsuka, J. Jpn. Mech. Eng. Int. 35 (1992) 82.

[20] W. He, Q. Chen, J. Power Sources 55 (1995) 25–32.

[21] F. Yoshiba, N. Ono, Y. Izaki, T. Watanabe, T. Abe, J. Power sources 71 (1998) 328–335.

[22] W. He, Q. Chen, J. Power Sources 73 (1998) 182–192.

[23] Y.R. Lee, I.G. Kim, G.Y. Chung, C.G. Lee, H.C. Lim, T.H. Lim, S.W. Nam, S.A. Hong, J. Power Sources 137 (2004) 9–16.

[24] B. Marcenerro, F. Federici, Proceedings of the International Hydrogen Energy Congress and Exhibition, pap. FCD244, 23-15, Istanbul, Turkey, 2005.

[25] F. Standeart, K. Hemmes, N. Woudstra, J. Power Sources 63 (1996) 221–234.

[26] M. Baranak, H. Atakül, T. Şener, F. Akgün, M. Tırıs, Proceedings of the International Hydrogen Energy Congress and Exhibition, pap. FCD272, 23-15, Istanbul, Turkey, 2005.

[27] C. Hitchings, Fuel Cell Handbook, Sixth Ed., EG&G Technical Services, Inc., Virginia, 2002.

[28] H. Morita, M. Komoda, Y. Mugikura, Y. Izaki, T. Watanabe, Y. Masuda, T. Matsuyama, J. Power Sources 112 (2002) 509–518.

[29] A. Weber, R. Darling, J. Meyers, J. Newman, in: W. Vielstich, A. Lamm, H.A. Gasteiger (Eds.), Handbook of Fuel Cells, Fundamentals, Technology and Applications, vol. 1, Wiley, New York, 2003, pp. 47–69.

[30] E. Arato, B. Bosio, P. Costa, F. Parodi, J. Power Sources 102 (2001) 74–81.